Earth Surface Processes and Landforms
Earth Surf. Process. Landforms **30**, 305–323 (2005)
Published online in Wiley InterScience (www.interscience.wiley.com). **DOI:** 10.1002/esp.1143

Large landslides and their effect on sediment flux in South Westland, New Zealand

Oliver Korup
School of Earth Sciences, Victoria University of Wellington, PO Box 600, New Zealand

**Correspondence to: O. Korup, WSL Swiss Federal Institute for Snow and Avalanche Research SLF, CH-7260 Davos, Switzerland. E-mail: korup@slf.ch*

Received 9 January 2004;
Revised 5 May 2004;
Accepted 19 July 2004

Abstract

Landslides and runoff are dominant erosional agents in the tectonically active alpine South Westland area of New Zealand, characterized by high uplift rates and extreme orographic precipitation. Despite a high density of shallow debris slides and flows, the geomorphic imprints of deep-seated bedrock failures are dominant and persistent. Over 50 large (>1 km^2) landslides comprising rock slide/avalanches, complex rotational and rock-block slides, wedge failures, and deep-seated gravitational slope deformation were detected on air photos and shaded-relief images. Major long-term impacts on alpine rivers include (1) forced alluviation upstream of landslide dams, (2) occlusion of gorges and triggering of secondary riparian landslides, and (3) diversion of channels around deposits to form incised meandering gorges. Remnants of large prehistoric (i.e. pre-1840) landslide deposits possibly represent the low-frequency (in terms of total area affected yet dominant) end of the spectrum of mass wasting in the western Southern Alps. This is at odds with high erosion rates in an active erosional landscape. Large landslides appear to have dual roles of supplying and retaining sediment. The implications of these roles are that (1) previous models of (shallow) landslide-derived sediment flux need to be recalibrated, and (2) geomorphic effects of earthquake-induced landsliding may persist for at least 10^2 years.

Keywords: landslide; sediment delivery; sediment flux; aggradation; New Zealand

Introduction

Detection and mapping of large landslides can be used for geomorphic hazard assessments, estimates of erosion and sediment discharge, and protection of settlements and infrastructure (Whitehouse and Griffiths, 1983; Eisbacher and Clague, 1984; Davies and Scott, 1997; Shroder and Bishop, 1998; Fort, 2000). High-magnitude earthquakes play an important role as preparatory and triggering variables for landslides (Keefer, 1999), reducing slope stability through rock shattering, fault zone weakening, slope tilting, or topographic amplification of ground shaking (Hancox *et al*., 1997). Direct physical impact from long-runout landslides and geomorphic long-term effects of post-earthquake aggradation in mountain rivers (Pain and Bowler, 1973; Pearce and Watson, 1986) pose significant hazards and risks to settlements and land use not only at, but also up- and downstream of failure sites (Davies and Scott, 1997; Korup, 2003). Typical off-site effects relating to landslide-induced aggradation include coarse floodplain deposition, channel instability, large-scale avulsion (Hancox *et al*., 1999), and increased flood frequency. Gauging the fluvial response and morphologic adjustment to excessive debris input, in terms of channel changes and sediment discharge, requires detailed information from landslide-affected catchments. In this regard, the role of large landslides in alpine sediment flux has so far received little attention (Korup *et al*., 2004). Consequently, the objectives of this study are

- to semi-quantitatively describe and characterize large landslides in the western Southern Alps;
- to reconstruct the geomorphic impact of these landslides on river channels and valley-floors; and
- to assess the role of large landslides in regional sediment flux with respect to large earthquakes.

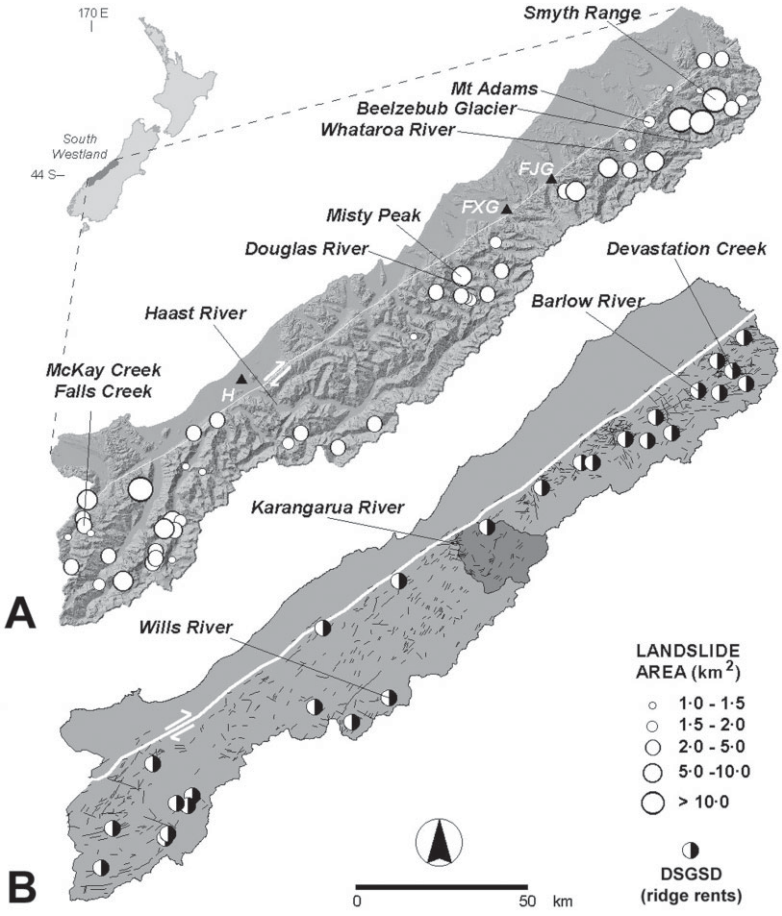

Figure 1. Maps of South Westland between Waitaha and Cascade Rivers, to the north and south, respectively. Tasman Sea bounds study area to the NW, and the main divide of the Southern Alps to the SE. (A) Shaded relief and location of large (>1 km^2) alpine landslides. (B) Major geological lineaments (>1 km), ridge rents, and DSGSD (deep-seated gravitational slope deformation; Agliardi *et al.*, 2001). White line indicates trace of Alpine Fault; FJG, Franz Josef Glacier (Township); FXG, Fox Glacier (Township); H, Haast.

Regional Setting

The study area of alpine South Westland lies between the Waitaha and Cascade Rivers to the west of the main divide of the Southern Alps (42°57′–44°30′ S, 168°16′–170°56′ E; Figure 1). The NW boundary is the Alpine Fault, which marks the oblique convergence between continental crusts of the Indo-Australian and Pacific plates. Active dextral transpressional movement along this major boundary leads to crustal shortening and uplift of the Southern Alps orogen. Inferred interplate velocities are *c*. 37 ± 2 mm a^{-1} during the last 3 Ma, *c*. 75 per cent of which are accommodated as strike- and dip-slip along the Alpine Fault (Norris and Cooper, 2000). Rapid uplift along the fault has exhumed quartzofeldspathic schist of the Haast Group of up to amphibolite/garnet-oligoclase metamorphic grade on the hanging wall, from depths of 20–25 km (Norris and Cooper, 1997). In the southernmost areas lithology is dominated by ultramafic rocks of the accreted and fault-deformed Dun Mountain–Maitai terrane (Bishop, 1994; Turnbull, 2000). The Southern Alps are exposed to moisture-laden northwesterly airflow, and receive orographically enhanced precipitation of up to 14 000 mm a^{-1} near the main divide (Henderson and Thompson, 1999). Erosion by frequent landsliding (Hovius *et al.*, 1997) and fluvial incision has created an asymmetric range cross-section. The Southern Alps are characterized by rectilinear slopes, serrated ridges, and intensely dissected valley sides with modal slopes of 38–40°, drained by steep and closely spaced mountain rivers. Most of the hillslopes <1000 m a.s.l. sustain dense stands of forest. The Alpine Fault separates the mountain range from a narrow subdued foreland of early

Palaeozoic basement covered by thick sequences of Pleistocene fluvioglacial outwash and large lateral moraine ridges and plateaux. At present, 11 per cent of the study area is glaciated. Estimates of erosion rates and offshore deposition suggest balanced rates of uplift and denudation of up to *c*. 11 mm a^{-1} (Basher *et al*., 1988; Hovius *et al*., 1997; Walcott, 1998). Despite the high degree of neotectonic activity in New Zealand, the South Westland area has historically experienced little major seismicity (Eberhardt-Phillips, 1995). Recent palaeoseismological studies recognized three $M = 8 \pm 0{\cdot}25$ earthquakes on the Alpine Fault during the last 1000 years (Wells *et al*., 2001; Yetton *et al*., 1998; Norris *et al*., 2001).

Previous Work

Large landslides are scattered throughout the Southern Alps, but are rarely documented in South Westland. Whitehouse (1983) investigated 42 rock avalanches in the central Southern Alps and estimated their respective sediment yield at 100 t km^{-2} a^{-1} during the last 2 ka. Whitehouse and Griffiths (1983) estimated return periods of 92 years on average for rock avalanches >10^6 m^3. However, four large (>10^6 m^3) rock avalanches occurred in the 1990s alone (Hancox *et al*., 1999; McSaveney, 2002), suggesting return periods near the main divide of 20–30 years (McSaveney, 2002). Hovius *et al*. (1997) mapped *c*. 5000 shallow aseismic landslides in the northern half of the study area. Accounts of large (>1 km^2), deep-seated landslides, however, remain at reconnaissance stage (Bishop, 1994; Hancox *et al*., 1997; Yetton *et al*., 1998). Beck (1968) described ridge rents and gravity faulting in the area of Wanganui River. Whitehouse (1986, 1988) commented on large (*c*. 10^8 m^3), extremely slow-moving 'mountain-slides' (Bishop, 1994; Prebble, 1995). Wright (1999) described catastrophic long-runout debris avalanche deposits, covering *c*. 5 km^2 of the central Westland piedmont near Hokitika. Hancox *et al*. (1999) gave a detailed account on the 1999 Mt Adams rock avalanche ($10–15 \times 10^6$ m^3), which formed a temporary landslide dam on Poerua River. Korup *et al*. (2004) estimated the resulting post-failure sediment budget and compared it with other historic events in the Southern Alps. Korup and Crozier (2002) described three large landslides and their geomorphic impact on mountain rivers, and noted the research gap on large landslides in the area.

Methods

A regional reconnaissance of >3000 air photos was conducted to identify and map large landslides in South Westland (Korup, 2003). Locations of slope instability were treated as tentative until validated by either sequential air photos, published data, or field study. Key diagnostics for assigning landslide type (Cruden and Varnes, 1996) were based on morphologic interpretation of headscarps and associated deposits. A 25-m grid digital elevation model (DEM) aided interpretation and mapping using shaded relief with varying illumination angles, extraction of surface profiles, and estimates of eroded landslide volumes with cut-and-fill algorithms. Soeters and Van Westen (1996) summarize methods, problems and limitations of GIS-based mapping of mass movements from air photos. Landslide morphometry was partly inferred and adapted from digital topographic data at 1:50 000 scale (Land Information New Zealand, 2000), and augmented from entries in a national landslide inventory (G. Dellow, pers. comm., 2002). Fieldwork mainly consisted of visiting selected features and examining morphostratigraphic exposures. Thus verified, large landslides were digitized as polygons onto the DEM at 1:50 000 scale with a mapping resolution of <100 m. Landslide morphometric variables were extracted by standard GIS queries. Geological maps and reports were compiled from a variety of sources (Grindley, 1978; Craw, 1984; Hanson *et al*., 1990; Bishop, 1994; Turnbull, 2000; Turnbull *et al*., 2001; White, 2002).

Large Landslides and their Geomorphic Impact on River Systems

The visually dominant slope failures on forested hillslopes of the area are thousands of rapid debris slides and debris flows (landslide terminology follows Cruden and Varnes, 1996). These are shallow features with volumes of 10^2 to 10^5 m^3, often referred to as 'debris avalanches' (Whitehouse, 1986). Close inspection of air photography and shaded relief images revealed 52 large landslides with planform areas >1 km^2 (Figure 1). They are predominantly deep-seated and complex, and affect a total area of 230 km^2, i.e. 4 per cent of the study area. The cumulative size distribution of log-transformed landslide area is linear over almost 1·5 orders of magnitude (Figure 2A). The landslides >1 km^2 vertically extend between 700 and 1900 m (Figure 2B), and have runout lengths between 1·5 and 5·6 km (Figure 2C). In total, >84 km of alpine trunk drainage are directly affected by these landslides; individual reach lengths affected by

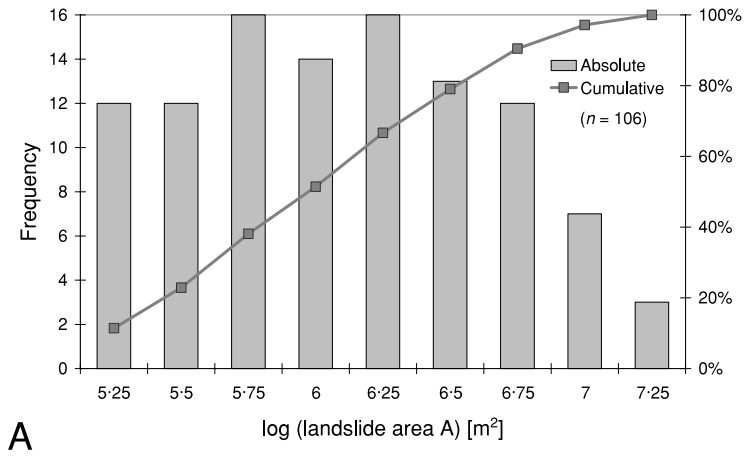

A

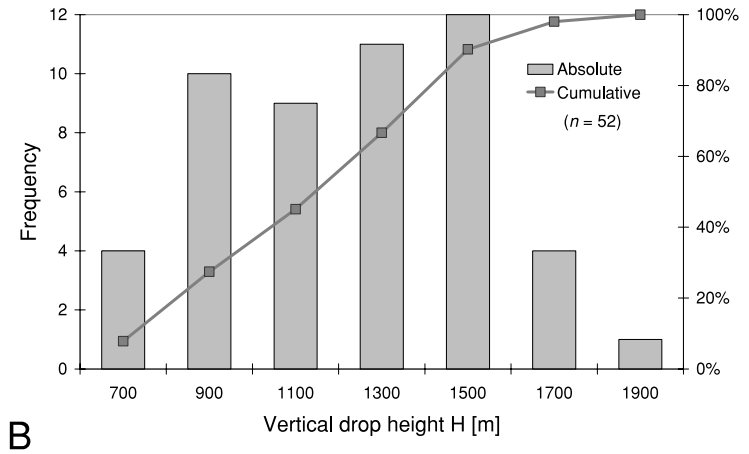

B

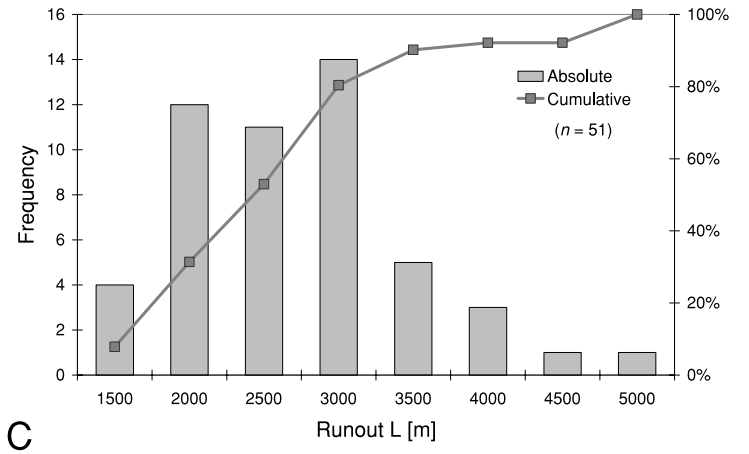

C

Figure 2. Histograms and cumulative distributions of landslides in alpine South Westland. (A) Landslide area for occurrences $>10^5$ m^3. (B) Vertical drop height (landslides $>10^6$ m^3). (C) Runout (landslides $>10^6$ m^3).

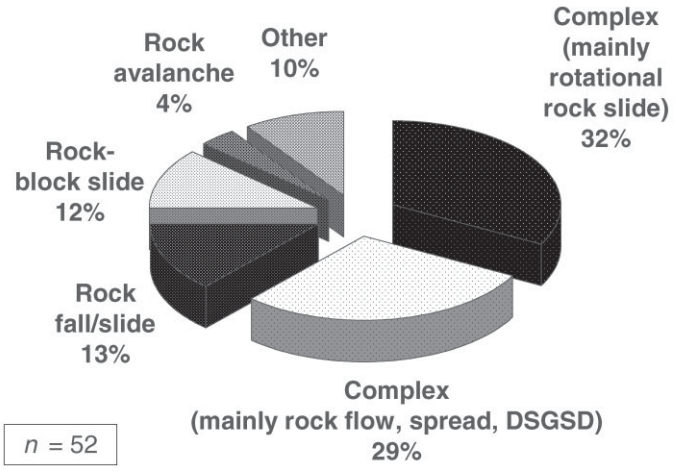

Figure 3. Types of large (>1 km^2) landslides in alpine South Westland (terminology follows Cruden and Varnes, 1996); dominant modes of failure are bracketed.

landslide deposits range between 0·5 and 10 km. Complex rotational rock slides (32 per cent), and complex rock flows and spreads (29 per cent) constitute the most frequent types of failure, followed by rock falls/slides, block slides, and rock avalanches (Figure 3).

The potential causes of large-scale bedrock landsliding include:

(1) stress release by slope de-buttressing following deglaciation or fluvial incision;
(2) slope dilatation following unloading by precursory landsliding and gradual reduction of the internal angle of friction;
(3) cumulative earthquake-induced weakening of rock-mass strength; or simply
(4) gravitational stress.

Earthquake shaking, fluvial incision, and high-intensity rainstorms including snowmelt processes are the most likely trigger mechanisms, whereas large rock flows and spreads respond to gravitational stress. The following section presents examples of selected landslide types, and examines their geomorphic effects on the drainage and sediment flux.

Rock avalanches

Rock avalanching is the extremely rapid flow movement of large volumes (>10^6 m^3) of catastrophically displaced and highly comminuted bedrock. Most rock avalanches in the Southern Alps have been recorded in Torlesse greywacke lithology east of the main divide (Whitehouse, 1983; McSaveney, 2002), likely reflecting erosional censoring more than lithological predisposition (Table I). The high degree of rock fragmentation in rock-avalanche deposits produces easily eroded, very angular, poorly sorted, fine gravelly to sandy debris. Fluvial entrainment of rock-avalanche material can thus be rapid once the bouldery surface armour is breached. The 1999 Mt Adams rock avalanche (Hancox *et al*., 1999) discharged up to $2{\cdot}5 \times 10^6$ m^3 a^{-1} of sediment during the first two years following failure of the dam it had formed on the Poerua River (Korup *et al*., 2004). Subsequent aggradation and avulsion on the Poerua alluvial fan at the range front is causing ongoing destruction of farmland. Similarly, episodic slope instability of the *c*. 2000 year old Zig-Zag rock-avalanche deposit, which had blocked Otira River in central Westland, required the realignment of a major state highway (Ramsay, 2000).

Further rock avalanches were found in North and Central Westland (Wright, 1999; McSaveney *et al*., 2000; Table I). Yetton *et al*. (1998) described deposits of a long-runout (*c*. 2 km) 'debris avalanche' at McTaggart Creek, and inferred temporary blockage of Karangarua River (see Figure 9). Rock slide/avalanching onto valley glaciers has locally produced extensive supraglacial debris (Figure 4). Detachment areas of former rock avalanches are often fringed with large scree ramparts, whereas the associated deposits are commonly hummocky with longitudinal and/or transverse furrows (Whitehouse, 1983). These diagnostic features are present in McKay Creek, Cascade River, where a former rock slide/avalanche dam is inferred. There, an extensive hummocky valley-floor deposit descended *c*. 600 m from a now scree-mantled 0·3 km^2 detachment area, which undermines a larger deep-seated rotational failure (Table I).

Table I. Identified large rock and debris avalanches in the Westland region (including the study area of South Westland), New Zealand

Location	Catchment	Age*	Deposit area (km^2)	Deposit volume (10^6 m^3)	Vertical drop (m)	Runout (m)	Remarks	Key Reference
Falling Mountain	Otehake	*AD 1929*	2·5	55	1200	4500	Triggered by 1929 Arthur's Pass Earthquake	McSaveney *et al.* (2000)
Otira (Zig-Zag)	Otira	2000 ± 90	0·43	43	>1000	?	Former landslide dam	Ramsay (2000)
Hunts Creek I	Taipo	3600 ± 940	0·63	35	>700	?	Remnant deposit only	Whitehouse (1983)
Hunts Creek II	Taipo	2750 ± 710	0·21	4	>700	?	Remnant deposit only	Whitehouse (1983)
Geologist Creek	Lake Kaniere	550 ± 50	?	?	?	?	Remnant deposit only	Yetton *et al.* (1998)
Cropp River	Hokitika	363 ± 46	?	0·2	?	?	Remnant deposit only	Yetton *et al.* (1998)
Round Top	Kokatahi	950 ± 50	3·1	45	740	4500	'Debris avalanche' in mylonitic schist	Wright (1999)
Mt Adams	Poerua	*AD 1999*	1·6	10–15	1850	2800	Shallow (<10 m) rock avalanche	Hancox *et al.* (1999)
Beelzebub Glacier	Adams (Wanganui)	*post-AD 1980*	0·23	1–2	320	1000	Supraglacial rock slide/avalanche	This study
McTaggart Creek	Karangarua	320	?	?	?	2000	'Debris avalanche' in biotite schist	Yetton *et al.* (1998)
McKay Creek	Cascade	prehistoric (*pre-AD 1840*)	0·8	?	600	1500	Former landslide dam	This study

* Italic dates are historic, otherwise age is in ^{14}C-years BP

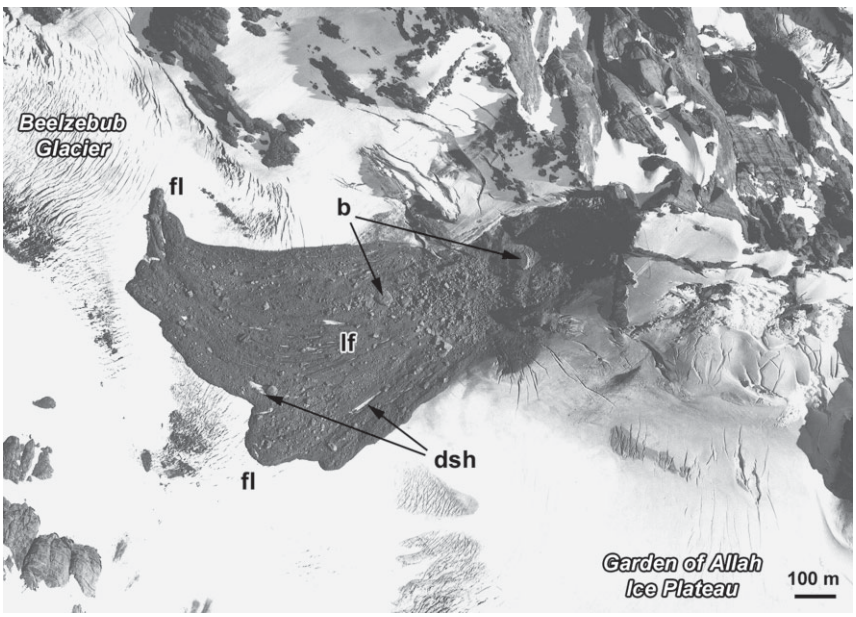

Figure 4. Rock slide/avalanche on Beelzebub Glacier, Garden of Allah Ice Plateau, upper Adams catchment (cf. Figure 1); fl, flow lobes, lf, longitudinal furrows; dsh, depositional shadows behind large boulders (b). Approximate scale only. Air photo courtesy of Land Information New Zealand (SNC8340/129 Crown Copyright reserved. Date: 12 Feb 1984).

The boulder-covered lobate debris appears to have swashed 160 m up on the opposite valley side, forming a *c.* 100 m high dam. The landslide forms a convex knickpoint in the long profile, and has forced alluviation upstream of the barrier. Downstream of the former landslide-dam crest, the stream has incised a 30–50 m deep meandering gorge into the landslide deposit (Figure 5A). Numerous other debris-mantled erosional scarps in the study area lack such distinctive flow-like debris mounds. These observations support the notion of rapid erosion of fragmented rock-avalanche debris from South Westland alpine rivers (Whitehouse, 1983).

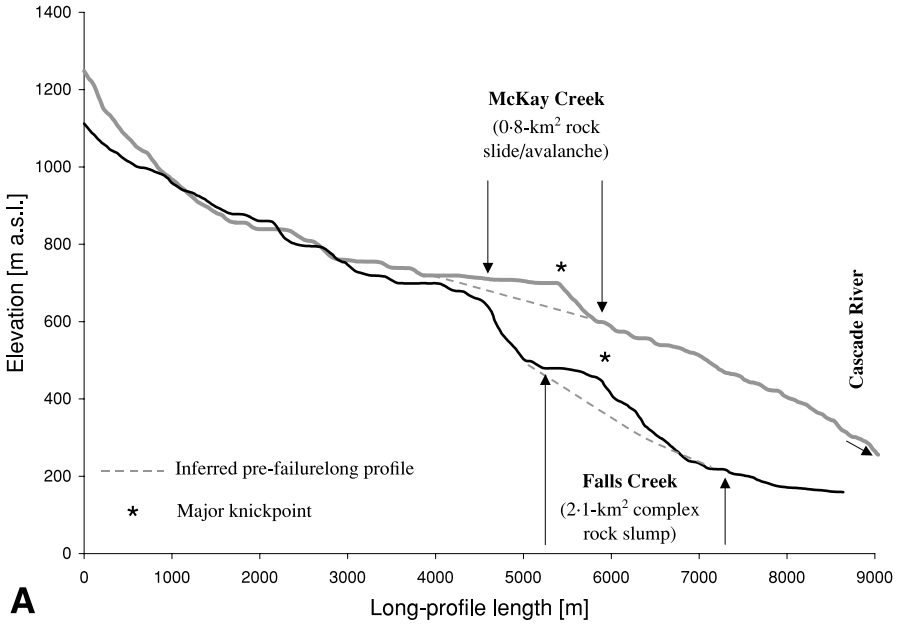

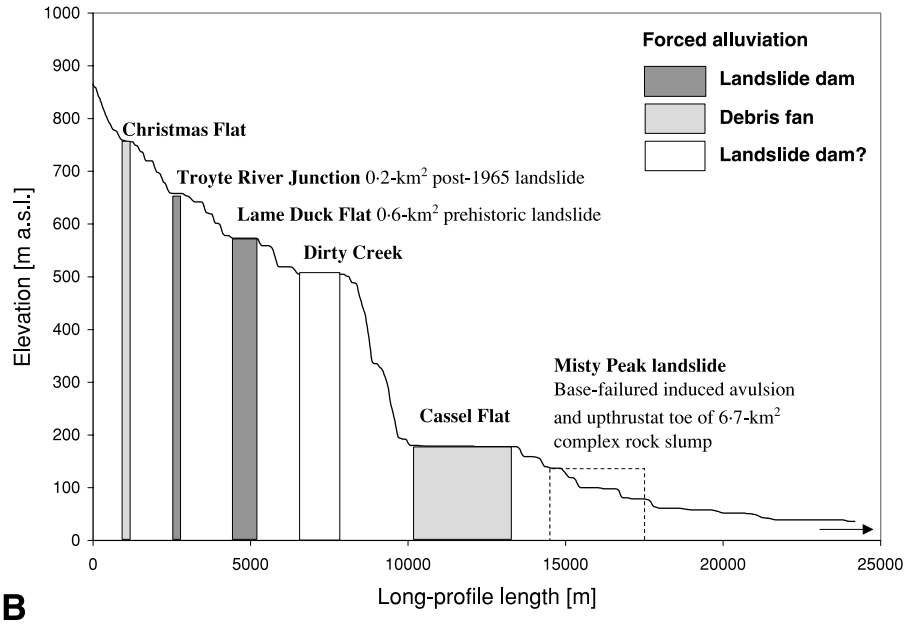

Figure 5. Landslide-induced disruption of river long profiles. (A) Reach-scale impact of large landslides at McKay and Falls Creeks, Cascade River (cf. Figure 1). (B) Forced alluviation upstream of landslide dams and debris fans leads to stepping of Karangarua River long profile.

Rock slide/wedge failures

Much of the drainage pattern in alpine South Westland is structurally controlled. The dominant NE trend of geological lineaments is subparallel to the Alpine Fault and general foliation of Haast schist (Hanson *et al*., 1990). Lineament mapping from the DEM showed that joint- or fault-controlled drainage axes of ravines and low-order tributaries often

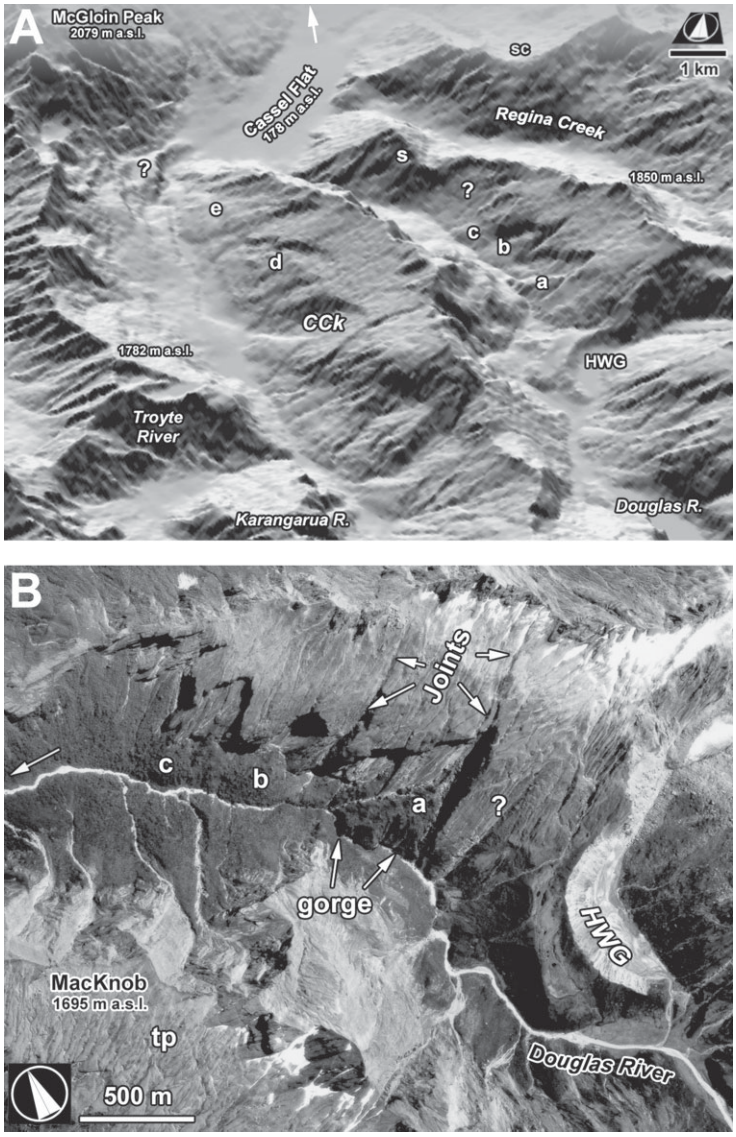

Figure 6. (A) Shaded relief image of upper Karangarua and Douglas Valleys: a–c, landslide deposits (debris cones had formed temporary blockage and subsequent occlusion of gorge); d,e, similar rock-slide deposits, including Coleridge Creek landslide (*CCK*); s, possible deep-seated failure; sc, crown scarp of Misty Peak landslide; ? indicates possible remnants of former landslides; HWG, Horace Walker Glacier. (B) Air photo detail of rock slide/wedge failures a–c; tp, surficial trapezoidal joints; ? indicates possible site of future failure. Approximate scale only. Air photo courtesy of Land Information New Zealand (SN8595/C10 Crown Copyright reserved).

connect across interfluves. The pattern of faults and joints is also an important control on slope stability. Almost 62 per cent of the large landslides identified intersect with lineaments >1 km in length (Figure 1).

Large deposits from structurally controlled wedge failures in schistose rock slopes have blocked the upper Karangarua River (Korup and Crozier, 2002). Similar cone-shaped deposits ($10–13 \times 10^6$ m^3) were found beneath prominent joint-bounded sigmoidal headscarps on the adjacent Douglas River (Figure 6). These rock slide/wedge failures occur in biotite/chlorite schist of N–S trending foliation and a dip of [040–050°]W near the Karangarua Syncline (Grindley, 1978). A trapezoidal fracture pattern is superimposed on major scarp-bounding joints of NE strike [020–075°] (Figure 6B). Rock slopes above the latero-frontal moraine wall of Horace Walker Glacier display a jointing pattern and mark a location for potential future failure (indicated by a question mark in Figure 6B). Based on air-photo interpretation,

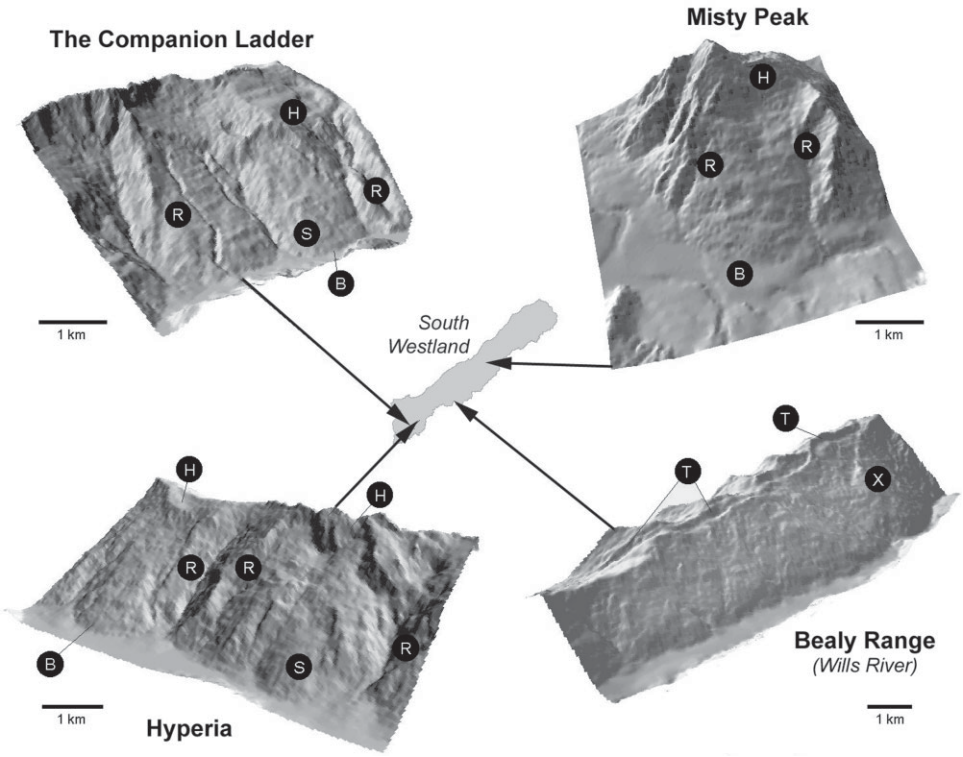

Figure 7. Diagnostic landforms of large deep-seated bedrock failures, including bulging slopes, pronounced smoothness, convex toe slopes, degree of dissection, ridge dislocation, and perched or lateral ravines; H, headscarp; R, perched lateral ravine; B, toe bulge; S, surficial rotational failure; T, ridge rent; X, fault or ridge rent.

large-scale jointing and intersecting planes of schistosity (Grindley, 1978) can be invoked as causes for this deep-seated slope instability, although the instability itself might relate to groundwater conditions.

The landslide deposits are littered with angular boulders, while partially detached rock slabs along the headscarps indicate sporadic rock slide and fall. Contour projections across the detachment area yield an estimated 33×10^6 m^3 source volume, suggesting that 30–40 per cent thereof has escaped erosion since failure. Cross-valley projection of the fluvially trimmed debris cones indicates former blockage of Douglas River, and subsequent incision of a *c*. 120 m deep meandering gorge around the deposit toe (labelled 'a' in Figure 6). A similar degree of erosion was observed at nearby Coleridge Creek (Korup and Crozier, 2002), where 40 per cent of some initial 62×10^6 m^3 rock-slide volume is preserved in the upper Karangarua valley (labelled '*CCk*' in Figure 6A).

Complex rock-block slides and slumps

Deep-seated complex bedrock failures comprising elements of rotational (block-)slide and flow movement are the most prevalent landslides in the study area (Figure 7). Shaded relief images were a powerful tool in identifying such failures, frequently characterized by displaced large intact rock blocks or slabs, conspicuous slope smoothness in otherwise dissected terrain, marked planform convexity of basal (diverted) channels, or bulging toe slopes. Distinctive head- and lateral scarps scoured by perched ravines, delineate these large features. Slope profiles are both convex and concave, and so are of limited use as morphologic indicators for slope instability (Figure 8). However, most deep-seated rotational failures exhibit slightly more subdued topography than that of their surrounding slopes.

An instructive example of a complex rock slide is situated at the confluence of Copland and Karangarua Rivers (Figure 9). Its pronounced crown scarp coincides with a *c*. 500 m headward dislocated ridge between Misty Peak and Cassel Hill (labelled 'sc' in Figure 6A), above 6·7 km^2 of irregular, hummocky terrain ($\varphi_{mod} = c.\ 22°$) in garnet/oligoclase schist (Grindley, 1978). The Misty Peak landslide comprises several tilted schist blocks that grade into transverse ridges and swales downslope. Asymmetric and complex slump features vertically extend over >1500 m. Subparallel pressure ridges bounding a slightly bulging terrace sequence on the true right of Karangarua River indicate

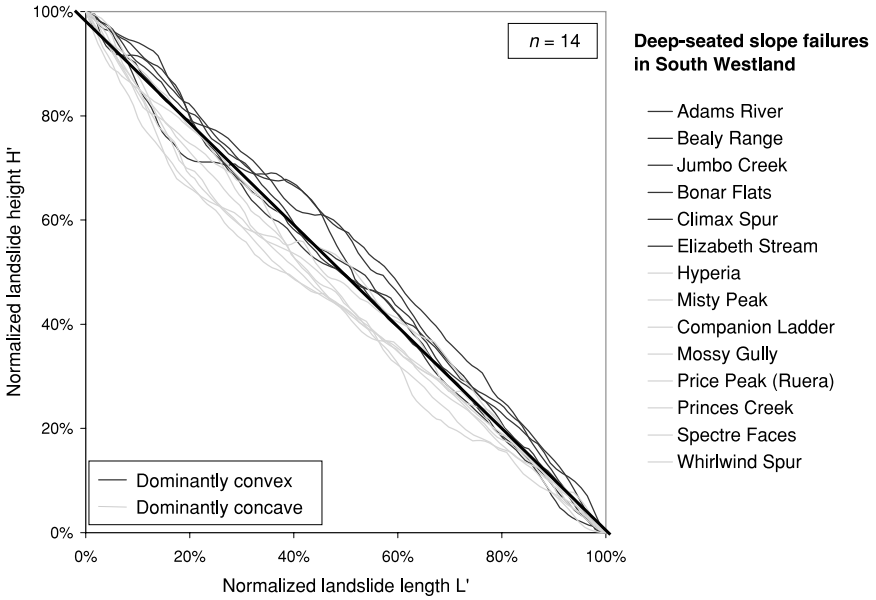

Figure 8. Plot of normalized height *H′* versus length *L′* for selected large (>1 km^2) deep-seated landslides in South Westland the 1:1 line indicates fully rectilinear slope long profile. Both slope concavity and convexity may be associated with major slope failures.

Table II. Geomorphometric properties of selected large mass movements in alpine South Westland

	Area (km^2)	Deposit volume (10^6 m^3)	Height (m)	Length (m)	Width (m)	Thick-ness (m)	Affected channel length (m)	Geomorphic impact
(a) Rock avalanches								
Mt Adams, Poerua River (Fig. 1)	1·6	10–15	1800	2700	1400	~10	1000	Temporary landslide dam, downstream aggradation
McKay Creek, Cascade River (Figs. 1, 5)	0·8	?	580	1500	700	?	1200	Temporary landslide dam, infilled lake?
(b) Complex deep-seated slumps								
Misty Peak, Karangarua River (Figs. 1, 9)	6·7	800	1500	3200	2300	120	?	Upthrust and avulsion
Falls Creek, Cascade River (Figs. 1, 5)	2·1	130	830	2300	1700	90	1800	Temporary landslide dam
(c) Rock slide/wedge failures								
Douglas River (Figs. 1, 6)	0·6	10–13	750	1300	850	30	900	Temporary landslide dam
Coleridge Creek, Karangarua River (Figs. 1, 6)	1·6	24	880	1800	1100	?	1200	Gorge occlusion, backwater alluviation
(d) Deep-seated gravitational slope deformation (DSGSD)								
Bealy Range, Wills River (Figs. 1, 7)	0·3	?	1100	2500	>1700	?	1850	Gorge occlusion
Smyth Range, Wanganui River (Figs. 1, 10)	>10	?	1540	4000	?	?	5500	Gorge occlusion?

movement at the landslide toe (Figure 9). Mature forest on the deposit suggests a minimum age of *c*. 200–300 years, i.e. prehistoric in New Zealand terms (pre-1840), although it may still be moving. Solifluction lobes and clusters of rock slabs nested below the headscarp, and distal flow structures indicate reactivation. Drainage patterns on the deposit indicate stream piracy in the wake of block sliding. DEM-based profile extraction yields conservative estimates of a deposit thickness of 100–150 m, and a landslide volume of *c*. 8×10^8 m^3 (Table II). The landslide affects the Karanguarua River bed, judging from an elevation difference of *c*. 20 m between an abandoned avulsion trace fringing the (visible) deposit toe and the present river channel (Figure 9). Base failure appears to have diverted the deformed fluvial

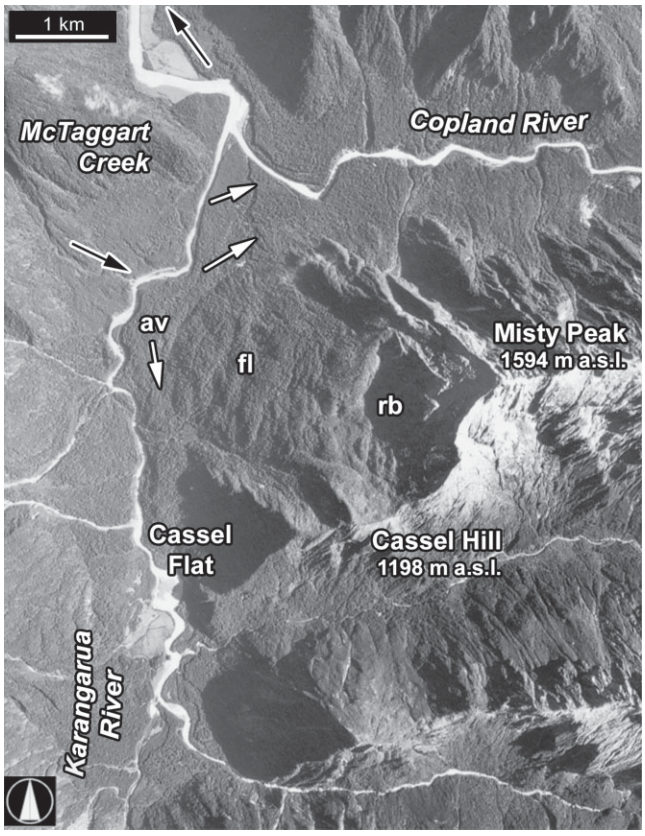

Figure 9. Deep-seated complex rotational rock slide/flow from Misty Peak, Copland/Karangarua River junction. White arrows depict Karangarua avulsion trace (av), now raised and indicated by terrace scarps; rb, partly rotated rock blocks; fl, secondary flow structure. Black arrow indicates former landslide dam formed by debris avalanche that issued from McTaggart Creek (Yetton *et al.*, 1998). Approximate scale only. Image courtesy of Land Information New Zealand (SN1708/D5 Crown Copyright reserved).

sediments at least twice. However, a landslide-driven valley-floor upthrust is not particularly evident in the river long profile, which is otherwise fragmented (Hewitt, 2002) by several landslides upstream (Figure 5B).

Several deep-seated complex rotational slides of similar size and morphology were mapped on NW-facing slopes, indicating a predisposing control of dip-slope schistosity planes on slope instability. Whitehouse (1986) described similar deep-seated rock-slope failures ($>10^{10}$ m^3) with crevassed, hummocky topography on planar slopes parallel to (pelitic) schistosity, possibly of Holocene or older age. Augustinus (1992) measured a one-third difference in point-load strengths parallel to foliation relative to those perpendicular to foliation in South Westland biotite schist, indicating a significant anisotropy in local rock-mass strength.

Deep-seated gravitational slope deformation (DSGSD)

The largest landslides in the area are *c.* 10^1 km^2 features of valley-side or headwall collapse. Accurate delineation and classification of these phenomena, variably termed deep-seated gravitational creep, sagging, or rock flow (Bisci *et al.*, 1996; Cruden and Varnes, 1996; Schmelzer, 2000), is difficult. 'Deep-seated gravitational slope deformation' (DSGSD; Agliardi *et al.*, 2001) is preferred here, since it does not imply movement rates. DSGSD in alpine South Westland is evident from numerous diagnostic morpho-structural landforms (Table III), and commonly extends beyond interfluves or catchment boundaries, thereby tilting or reorganizing low-order basins (labelled 's' in Figure 6A; Hovius *et al.*, 1998). Ridge rents (Beck, 1968; Grindley, 1978) were useful for detection on shaded relief images. Several ridge rents occur along the front range (Figure 1B) and may indicate tectonic nappe formation and subsequent gravity collapse in the Alpine Fault Zone (Simpson *et al.*, 1994).

The Price Range DSGSD (10–30 km^2), Whataroa River, exhibits headward ridge dislocation and extensional scree-mantled ridge-top basins. Surficial slump and flow deposits possibly occlude the lower Whataroa gorges, while a

Table III. Diagnostic morphostructural landforms of deep-seated gravitational slope deformation (DSGSD; Agliardi *et al*., 2001), compiled from Beck (1968), Radbruch-Hall (1978), Basher *et al*. (1988), Dramis and Sorriso-Valvo (1994), Prebble (1995), Bisci *et al*. (1996), Schmelzer (2000), and this study

Head slope	Mid-slope/toe slope	Valley floor
Displaced rows of rock pinnacles	Relocated bedding blocks	Bulging toe slopes Upthrust from base failures
Tilt- or truncation-induced stream piracy, retrogressive ridge migration	Subparallel pressure ridges	
Active scree and debris slopes		Distortion of valley-floor stratigraphy
'Saw-tooth' profile of counterscarps, ridge rents, and rock steps		
Serrated ridges and stepped ridge profiles	Recurrent fan-like bulging in homogeneous rock walls	Asymmetric occlusion (forcing gorge formation)
Headscarp fissures and (infilled) tension cracks, gullies, or depressions	Slope convexity	
Micro-graben structures and ridge-line depressions, double crests	Secondary nested rotational surface failures and toe-slope collapse features	
Dislocated and rotated intact rock blocks, flexural topple		
Terracettes		
Landslide ponds		Backwater aggradation

rectangular network of ravines is disrupted by offsets of interfluves (Figure 10A). Densely spaced, cross-cutting rents and faults may indicate large-scale tectonic denudation and brittle surface deformation. Characteristic valley cross-profiles of DSGSD show a convex (bulging) toe slope, causing gradual channel diversion and occlusion. Subsequent oversteepening of the juxtaposed toe-slope through fluvial undercutting triggers riparian landslides such as nested rotational bedrock failures (Figure 11).

Schistosity-parallel slopes of the Smyth Range, Wanganui River (Figure 10B), show strong structural segmentation and surficial dissection, possibly outlining individual fault blocks. The total area affected by DSGSD is *c*. 40 km^2, partly delineated by a large right-lateral scarp truncating the headwaters of Whirling Water in the adjacent Waitaha River catchment. The eastward continuation of this scarp is rather ill-defined. Major features include a *c*. 9 km^2 rotated triangular-shaped hillslope block with chaotic topography criss-crossed by partly tilted gullies. Terracettes, nested concentric scarplets, and surficial rotational slides indicate differential slope movements. Gently undulating ridge-mantling cirques and nivation hollows are truncated by a 40–60 m high counterscarp. Mid- to toe slopes are similarly segmented by several sets of subparallel rents for 6–8 km (Figure 10B), which form 190–240 m broad steps, dipping 48–58° N. Several 'blind' ravines suggest stream piracy following brittle slope deformation. Judging from general strike and sense of offsets these counterscarps may relate to a W–E trending population of dextral strike-slip faults in the nearby Waiho River (Hanson *et al*., 1990).

At present, movement rates of these DSGSD are unknown. Similar features in Haast Schist are well-known in central Otago, where they attain depths of 10^2 m, with movement assisted by high-pressure, perched water tables, and movement rates of up to 10^1 mm a^{-1} (Gillon *et al*., 1992) along dip-slope schistosity planes. Deep-seated creep at Carls Ridge above Hendes Creek, Wanganui River, showed historic acceleration of movement rates and rapid failure ('creep rupture'; Radbruch-Hall, 1978; Chigira and Kiho, 1994). There, gradual debuttressing caused rapid headscarp extension at 1·6–1·8 m a^{-1}, culminating in failure of a large (*c*. 8×10^6 m^3) complex rotational rock-block formerly truncated by ridge rents. The resulting debris formed large cones that temporarily blocked and infilled the valley-floor (Korup and Crozier, 2002).

Discussion

Large prehistoric landslides form important depositional landforms in the active erosional landscape of alpine South Westland. Catastrophic rock slide/avalanches and structurally controlled rock fall/wedge failures have formed temporary landslide dams, whereas deep-seated complex rotational rock slides and DSGSD divert channels or occlude valley floors to form gorges. The geomorphic significance of these large landslides for alpine sediment flux in the area depends on (a) their magnitude and frequency, (b) their possible relation to large earthquakes as trigger mechanisms, and (c) the residence time of their deposits.

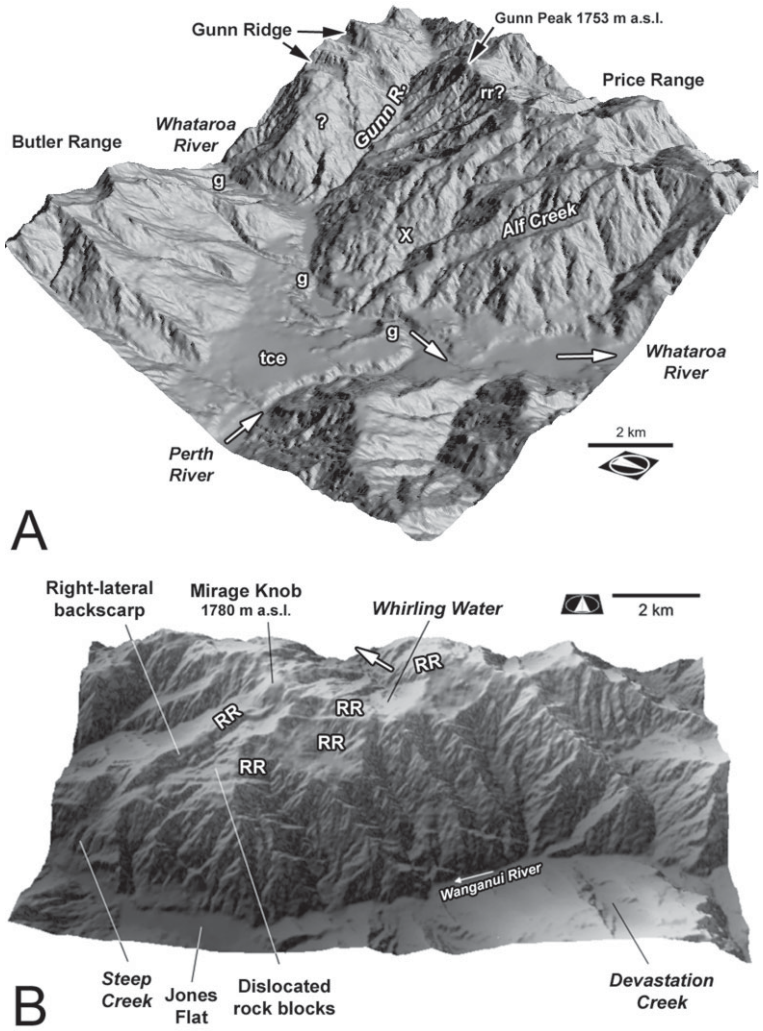

Figure 10. (A) Price Range, Whataroa River. Highly dissected hillslopes attest to erosive action of frequent shallow landsliding and fluvial dissection. Brittle surface deformation controls low-order drainage lines (X; Alf Creek); rr? ridge-truncating rents/faults. At Gunn Ridge are nested scree-mantled retrogressive tensional scarps (partially scoured by small cirque glaciers); ?, possible DSGSD; g, landslide-driven gorge occlusion; tce, valley fill (talus, alluvium). (B) Smyth Range, Wanganui River. Segmentation of hillslopes by ridge rents (RR) and fault scarps; note large right-lateral scarp and block-like displacement (cf. Figure 11C).

Magnitude and frequency

Hovius *et al*. (1997) modelled the annual probability of shallow aseismic landsliding <1 km^2 as a function of landslide area for 2670 km^2 of montane South Westland with a robust power-law function. Their data give an average density of *c*. 1·87 landslides km^{-2} for historic landslides (Table IV). Limited air photo counts suggest maximum values of 16–18 landslides km^{-2} near Franz Josef Glacier, coinciding with the area of greatest uplift of *c*. 10 mm a^{-1} (Figure 1; Norris and Cooper, 2000). Although the density of large (>1 km^2) landslides in South Westland is two orders of magnitude lower (0·01 landslides km^{-2}), the total area affected is nearly three times higher (Table IV). Thus the total area affected by landsliding is clearly dominated by large failures.

The model of Hovius *et al*. (1997) cannot be extrapolated to large landslides. Depending on the scaling exponents used ($\beta = 1{\cdot}16$ or 1·48; Hovius *et al*., 1997; Stark and Hovius, 2001), the annual exceedance probability (a.e.p.) for a landslide the size of the 1999 Mt Adams rock avalanche (*c*. 1·6 km^2) to occur in montane South Westland may be 0·072–0·084. This equals a return period T of 12–14 years. Air photo cross-checks indicate that such return periods are too short. Similarly, estimates of sediment production from landsliding possibly need recalibration. For example,

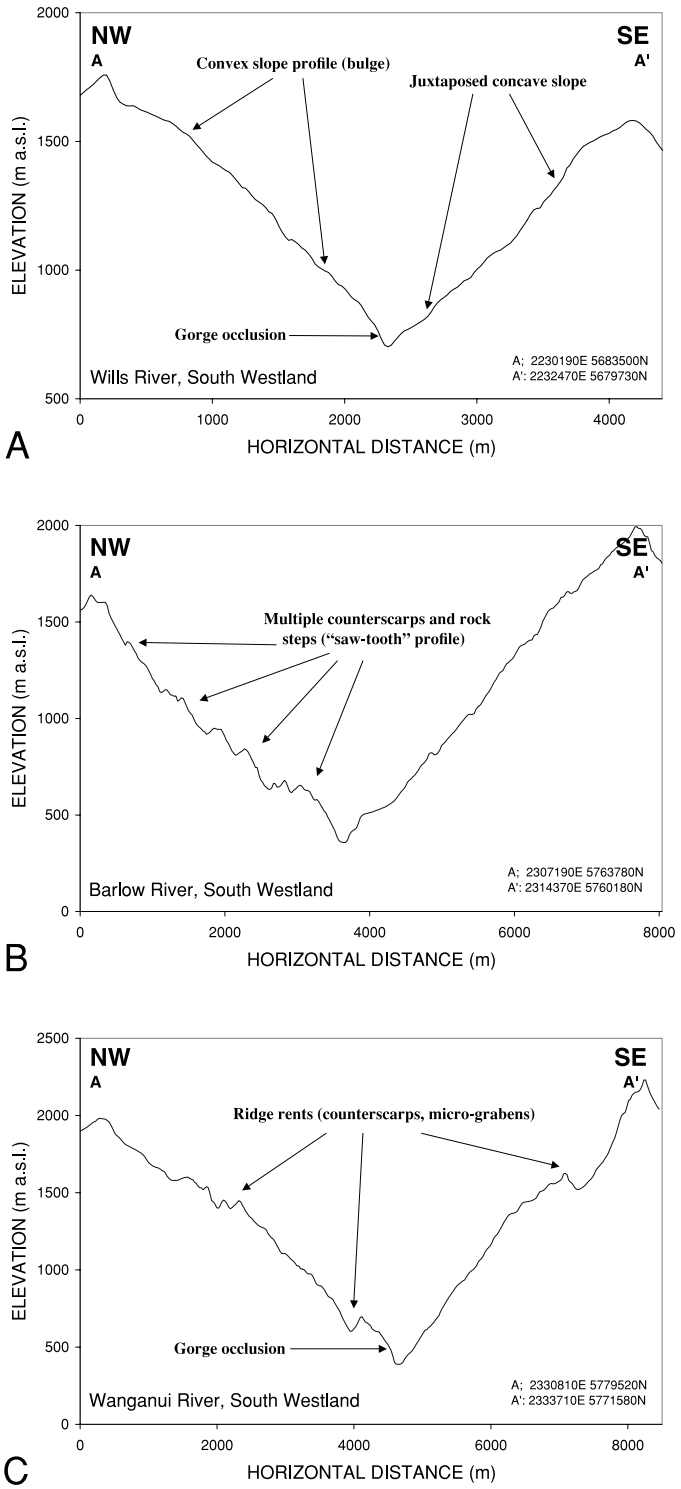

Figure 11. Asymmetric valley cross-profiles caused by DSGSD (exaggerated vertical scale). Affected slopes show ridge rents and counterscarps, bulging toes with associated channel deflection, juxtaposition of concave slopes, as well as 'saw-tooth' slope profiles. Note oversteepening of toe slopes by fluvial incision; coordinates refer to New Zealand Map Grid.

Table IV. Density of landsliding and total affected area in alpine regions of New Zealand

Region	*n*	Study area (km^2)	Total landslide area (km^2)	% of study area	Landslide density (km^{-2})	Minimum size (km^2)	Source
South Westland*	4984	2670	53	2·0	1·867	5×10^{-4}	Hovius *et al.* (1997)
South Westland*	25	2430	139	5·7	0·010	1	This study
South Westland†	52	5700	230	4·0	0·009	1	This study
Central Southern Alps‡	42	10000	35	0·4	0·004	1	Whitehouse (1983)

* Waitaha to Moeraki Rivers.

† Waitaha to Cascade Rivers (cf. Figure 1).

‡ Rock avalanches only.

adopting a (conservative) new upper length scale of landsliding at $L_1 = 2$ km would imply a regional denudation rate of 14 mm a^{-1} (Hovius *et al*., 1997). The model assumption of a balanced mass budget between landslide erosion and sediment export to the foreland may hold for small, shallow regolith landslides; it is less applicable though for large slope failures, which also induce major intramontane sediment storage. Magnitude/frequency relationships for large landslides cannot be established due to the lack of indication on age. Mature forest covers 52 per cent of the deposits on average and sets failure (or reactivation) ages to >200–300 years.

Earthquake-triggered landsliding and sediment production

Large landslides that are triggered or reactivated during large earthquakes are a major concern in hazard assessments within the region. The proximity of large, deep-seated bedrock failures to the Alpine Fault (<25 km) make prehistoric *M c*. 8 earthquakes plausible triggers (Yetton *et al*., 1998), although in many cases gravitational stress appears to be the motor of large-scale slope instability. Without detailed geotechnical stability analyses and with the possibility of various other trigger mechanisms (e.g. rainfall/snowmelt, fluvial undercutting), however, this notion is speculative (Crozier *et al*., 1995).

Catastrophic post-earthquake aggradation in rivers from landslide debris was inferred from the preservation of extraordinarily large amounts of woody debris in remnant terraces (Yetton *et al*., 1998). Adams (1979) noted that most of the 'abnormal' post-seismic sediment load in the Southern Alps might be carried out to sea in suspension in less than five years. Several studies attempted to quantify the sediment generated by coseismic landsliding: Keefer (1999) reviewed world-wide data and modelled average rates of >200 $m^3\ km^{-2}\ a^{-1}$ for the whole of New Zealand. Adams (1980) attributed half of the sediment production in the Southern Alps to earthquakes, e.g. $59 \times 10^6\ m^3$ to the 1929 Arthur's Pass Earthquake ($M_s = 6{\cdot}9$) in the central Southern Alps. Estimates of Hancox *et al*. (1997) of $100 \times 10^6\ m^3$ for the same event highlight the error margins in such studies. Estimates based on empirical formulas of Keefer (1999) suggest that *M c*. 8 earthquakes on the Alpine Fault could produce landslide debris of up to *c*. $10^9\ m^3$. With a return period of *c*. 250 years (Yetton *et al*., 1998), the resulting denudation rate of 0·2 mm a^{-1} through coseismic landsliding seems surprisingly low in comparison with rates of overall denudation. Moreover, the sequestration potential of large landslides, e.g. that at Misty Peak, which has retained a volume equivalent to that produced by eight major (1929 Arthur's Pass) earthquakes, or 615 years of sediment production from shallow landslides in the catchment (Hovius *et al*., 1997), is significant. It appears, that large-scale slope instability may locally counterbalance effects of post-earthquake aggradation. Understanding the geomorphic coupling and sedimentary link between landslides and alpine rivers is thus essential for assessing neotectonic landscape dynamics. This is particularly relevant to South Westland, where the observation window (*c*. 25 years) is an order of magnitude lower than the inferred recurrence interval of major earthquakes (*c*. 250 years).

Reservoir effects of large landslides in alpine sediment flux

Deep-seated landsliding (excluding DSGSD) is a substantial consequence of earthquakes. Despite numerous studies on coseismic landsliding worldwide, there is little quantitative work on post-earthquake sediment flux. The likely spectrum is indicated by work on the 1970 Papua New Guinea (Pain and Bowler, 1973), and the 1929 Murchison earthquakes in South Island, New Zealand (Pearce and Watson, 1986). In Papua New Guinea nearly half of the landslide-derived sediment had been cleared from the affected basins several years after the event. New Zealand catchments, however, retained about half of the debris in headwaters due to large calibre and sediment trapping in

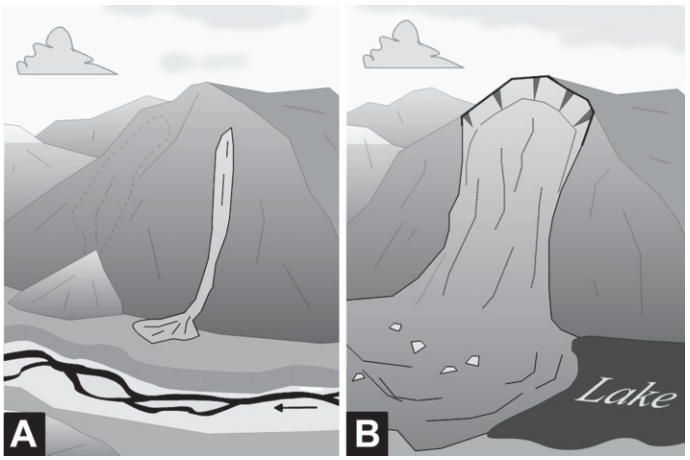

Figure 12. Concept of landslide-size-dependent 'thresholds' for sediment delivery to river channels. (A) Ratio of landslide runout to slope length and potential buffer width is insufficient to deliver sediment to the channel. (B) Landslide size in relation to cross-valley length scale is sufficient to overwhelm the channel and form a stable landslide-dammed lake.

several stable coseismic landslide dams. Owen *et al*. (1996) calculated sediment delivery ratios (SDRs) from landslides to be between 0·5 and 0·84, following the 1991 Garhwal earthquake in the Indian Himalayas. Depending on the topography of the landslide emplacement site, local historic SDRs may be <0·2 in the Southern Alps (Korup and Crozier, 2002; Korup *et al*., 2004). Such figures are biased by landslide deposits that survived for a long time, especially since it is difficult to estimate the amount of (totally) eroded landslide debris elsewhere. If we assume that a substantial number of landslides has shared this fate, further research needs to examine the controls on the prolonged residence time of some deposits.

Based on observations in the study area, it is argued that the relation between landslide and catchment morphometry controls sediment discharge from, and residence time of, landslide deposits. Two critical 'thresholds' of landslide size-dependent sediment discharge can be formulated (Figure 12).

(1) Landslides are too small to reach the drainage network (Figure 12A). This lower size-constrained sediment retention is controlled by hillslope length, flow obstacles, and valley-floor buffer zones. In the study area *c*. 9 per cent of rapid debris slides and flows are buffered from valley trains. In the case of the 1999 Chamoli earthquake in the Garhwal Himalaya, India, Barnard *et al*. (2001) recorded that *c*. 60 per cent of all coseismic shallow landslides did not enter streams.
(2) Landslides are large enough to form dams, thus disrupting or obliterating the drainage system (Figure 12B). Long-term blockage will force backwater alluviation and sediment trapping behind landslide dams or, in extreme cases, drainage reversal. This upper size-constrained sediment retention is controlled by valley geomorphometry, catchment size, and landslide dam dimensions.

Large landslides may also sequester debris from streams. For instance, base failure-induced upthrust and diversion of Karangarua River has helped to protect the Misty Peak deposit from fluvial erosion at the junction of two major alpine rivers (Figure 9). Large prehistoric landslide deposits on toe slopes and valley floors indicate the dominance of fluvial downcutting over lateral erosion, and thus limited evacuation of debris. Incision is enhanced by landslide-driven gorge occlusion (including valley-floor uplift) or blockage, forcing backwater alluviation and stepping of the river longitudinal profile (Figure 5). Multiple landslide dams form cascading sediment storages, initially described for the Karakoram Himalayas (Hewitt, 2002). Such landslide-driven river fragmentation may be an important control in many other mountain rivers (Fort, 2000; Maas and Mackin, 2002; Korup, 2003). Failure or breaching of landslide dams, however, favours increased sediment flushing following catastrophic outburst floods. Interestingly, Schlunegger (2002) concluded from catchment-scale channel-hillslope diffusivity models in the Swiss Alps, that high sediment delivery from hillslopes caused the formation of steps in the stream long profiles, through increased valley-floor aggradation, and decreased sediment export from the basin.

Based on the simplistic model of landslide-size-dependent sediment retention (Figure 12) it is argued that large landslides in alpine South Westland may both produce and retain large volumes of sediment. Their geomorphic significance thus encompasses at least partial regulation of catchment sediment flux.

Conclusions

The size range of large landslides in the western Southern Alps extends to 10^1 km^2 and comprises deep-seated complex failures, deep-seated gravitational slope deformation, and possibly large-scale features of tectonic denudation. Major geomorphic long-term impacts on alpine rivers include (1) forced alluviation upstream of landslide dams, (2) occlusion of gorges and triggering of secondary riparian landslides, and (3) diversion of channels around deposits, causing incision of meandering gorges. The preservation of large prehistoric landslide deposits in the active erosional landscape suggests that medium-term sediment delivery ratios from these sites are rather low. This applies to deep-seated rotational and rock-block slides, whereas highly fragmented rock-avalanche debris is more rapidly evacuated. However, no quantitative estimates exist on the material lost from deposits that were fully eroded. Size-constrained buffering as well as size-induced long-term disruption or obliteration of valley floors may efficiently preclude or decelerate erosion of landslide debris. It should thus not be surprising to detect coseismic landslide deposits from the last Alpine Fault earthquake (AD 1717; Yetton *et al*., 1998) in the study area, although none have been identified to date.

Landslide-driven sediment retention may affect sediment flux from mountain belts on time scales of up to 10^4 years; or possibly even longer (Fort, 2000). This regulatory role of hillslope processes deserves more attention in orogen-scale mass-balance models assuming steady-state conditions (Hovius *et al*., 1997). The landslide-driven initiation of knickpoints in river long profiles also can mask or mimic the effect of tectonic forcing. Burbank and Anderson (2001) noted that high residence times of large landslide deposits can distort geochemical isotope signatures in fluvial sediments, thus complicating studies on provenance or erosion rates.

Further work is required to investigate landslide-driven sediment storage. It is pertinent to query which band in the magnitude–frequency spectrum of landsliding achieves the highest geomorphic work in terms of erosion and sediment delivery in the long term: few large catastrophic landslides or numerous smaller landslides? In the Nepal Himalaya, Fort (2000) related the spatial distribution of large intramontane alluvial flats to landslide dams, which have existed for 10^4 years. In contrast, single landslides can produce peaked sediment pulses well in excess of long-term basin yield (Ries, 2000). Gerrard and Gardner (2000) stressed the importance of large landslides in the Middle Hills of Nepal, which apart from shaping the landscape, have also pre-conditioned the location of small shallow failures. Reflecting on the examples presented in this study it appears that this statement also applies to the western slopes of the Southern Alps.

Acknowledgements

Thanks are due to Mike Crozier for his constant support. Much of this study was financed by a Victoria University of Wellington Postgraduate Scholarship. Grant Dellow, Nick Perrin, and Mauri McSaveney, Institute of Geological and Nuclear Sciences, Lower Hutt, NZ, kindly provided site-specific landslide data. Niels Hovius and Colin Stark are thanked for making accessible their data set. Constructive comments by Mauri McSaveney and an anonymous reviewer were greatly appreciated.

References

Adams JE. 1979. Sediment loads of North Island rivers, New Zealand – a reconnaissance. *Journal of Hydrology (New Zealand)* **18**: 36–48.

Adams JE. 1980. Contemporary uplift and erosion of the Southern Alps, New Zealand. Part 2. *Geological Society of America Bulletin* **91**: 1–114.

Agliardi F, Crosta G, Zanchi A. 2001. Structural constraints on deep-seated slope deformation kinematics. *Engineering Geology* **59**: 83–102.

Augustinus PC. 1992. The influence of rock mass strength on glacial valley cross-profile morphometry: a case study from the Southern Alps, New Zealand. *Earth Surface Processes and Landforms* **17**: 39–51.

Barnard PL, Owen LA, Sharma MC, Finkel RC. 2001. Natural and human-induced landsliding in the Garhwal Himalaya of northern India. *Geomorphology* **40**: 21–35.

Basher LR, Tonkin PJ, McSaveney MJ. 1988. Geomorphic history of a rapidly uplifting area on a compressional plate boundary: Cropp River, New Zealand. *Zeitschrift für Geomorphologie Supplementband N.F.* **69**: 117–131.

Beck AC. 1968. Gravity faulting as a mechanism of topographic adjustment. *New Zealand Journal of Geology and Geophysics* **11**: 191–199.

Bisci C, Dramis F, Sorriso-Valvo M. 1996. Rock flow (sackung). In *Landslide Recognition. Identification, Movement and Causes*, Dikau R, Brunsden D, Schrott L, Ibsen ML (eds). John Wiley: Chichester; 150–160.

Bishop DG. 1994. *Geology of the Forgotten River area*. Institute of Geological and Nuclear Sciences Geological Map 15. Lower Hutt.

Burbank DW, Anderson RS. 2001. *Tectonic Geomorphology*. Blackwell Science: Malden, MA.

Chigira M, Kiho K. 1994. Deep-seated rockslide-avalanches preceded by mass rock creep of sedimentary rocks in the Akaishi Mountains, central Japan. *Engineering Geology* **38**: 221–230.

Craw D. 1984. Lithologic variations in Otago Schist, Mt Aspiring area, northwest Otago, New Zealand. *New Zealand Journal of Geology and Geophysics* **27**: 151–166.

Crozier MJ, Deimel MS, Simon JS. 1995. Investigation of earthquake triggering for deep-seated landslides, Taranaki, New Zealand. *Quaternary International* **25**: 65–73.

Cruden DM, Varnes DJ. 1996. Landslide types and processes. In *Landslides: Investigation and Mitigation*, Turner AK, Schuster RL (eds). Special Report 247. Transportation Research Board, National Research Council: 36–75.

Davies TRH, Scott BK. 1997. Dambreak flood hazard from the Callery River, Westland, New Zealand. *Journal of Hydrology (New Zealand)* **36**: 1–13.

Dramis F, Sorriso-Valvo M. 1994. Deep-seated gravitational slope deformation, related landslides and tectonics. *Engineering Geology* **38**: 231–243.

Eberhardt-Phillips D. 1995. Examination of seismicity in the central Alpine Fault region, South Island, New Zealand. *New Zealand Journal of Geology and Geophysics* **38**: 571–578.

Eisbacher GH, Clague JJ. 1984. *Destructive mass movements in high mountains: hazard and management*. Geological Survey of Canada Paper 84-16.

Fort M. 2000. Glaciers and mass wasting processes: their influence on the shaping of the Kali Gandaki valley (higher Himalaya of Nepal). *Quaternary International* **65/66**: 101–119.

Gerrard AJ, Gardner RAM. 2000. The role of landsliding in shaping the landscape of the Middle Hills, Nepal. *Zeitschrift für Geomorphologie Supplementband* N.F. **122**: 47–62.

Gillon MD, Denton BN, Macfarlane DF. 1992. Field investigation of the Cromwell Gorge landslides. In *Landslides. Glissements de terrain*, Bell DH (ed.). Proceedings of the 6th International Symposium, 10–14 February 1992, Christchurch. Balkema: Rotterdam; 707–713.

Grindley GW. 1978. Alpine Schist Belt – Haast to Wanganui Rivers, South Westland. In *The Geology of New Zealand*, Suggate RP, Stevens GR, Te Punga MT (eds). Government Printer: Wellington; 297–301.

Hancox GT, Perrin ND, Dellow GD. 1997. *Earthquake-induced landsliding in New Zealand and implications for MM intensity and seismic hazard assessment*. GNS Client Report 43601B prepared for Earthquake Commission Research Foundation: Lower Hutt.

Hancox GT, McSaveney MJ, Davies TR, Hodgson K. 1999. *Mt Adams rock avalanche of 6 October 1999 and subsequent formation and breaching of a large landslide dam in Poerua River, Westland, New Zealand*. Report 99/19. Institute of Geological and Nuclear Sciences: Lower Hutt.

Hanson CR, Norris JR, Cooper AF. 1990. Regional fracture-patterns east of the Alpine Fault between the Fox and Franz Josef Glaciers, Westland, New Zealand. *New Zealand Journal of Geology and Geophysics* **33**: 617–622.

Henderson RD, Thompson SM. 1999. Extreme rainfalls in the Southern Alps of New Zealand. *Journal of Hydrology (New Zealand)* **38**: 309–330.

Hewitt K. 2002. Postglacial landform and sediment associations in a landslide-fragmented river system: the Transhimalayan Indus streams, Central Asia. In *Landscapes of Transition*, Hewitt K (ed.). Kluwer: Amsterdam; 63–91.

Hovius N, Stark CP, Allen PA. 1997. Sediment flux from a mountain belt derived from landslide mapping. *Geology* **25**: 231–234.

Hovius N, Stark CP, Tutton MA, Abbott LD. 1998. Landslide-driven drainage network evolution in a pre-steady-state mountain belt: Finisterre Mountains, Papua New Guinea. *Geology* **26**: 1071–1074.

Keefer DK. 1999. Earthquake-induced landslides and their effects on alluvial fans. *Journal of Sedimentary Research* **69**: 84–104.

Korup O. 2003. *Landslide-induced river disruption – Geomorphic imprint and scaling effects in alpine catchments of South Westland and Fiordland, New Zealand*. PhD thesis, Victoria University of Wellington.

Korup O, Crozier M. 2002. Landslide types and geomorphic impact on river channels, Southern Alps, New Zealand. In *Landslides*, Rybar J, Stemberk J, Wagner P (eds). Proceedings 1st European Conference on Landslides, 24–26 June 2002, Prague. Balkema: Rotterdam; 233–238.

Korup O, McSaveney MJ, Davies TRH. 2004. Sediment generation and delivery from large historic landslides in the Southern Alps, New Zealand. *Geomorphology* **61**: 189–207.

Land Information New Zealand. 2000. *25-m Digital Elevation Model based on NZMS260 digital 20-m contours (scale 1:50 000)*. Land Information New Zealand: Wellington.

Maas GS, Macklin MG. 2002. The impact of recent climate change on flooding and sediment supply within a Mediterranean mountain catchment, southwestern Crete, Greece. *Earth Surface Processes and Landforms* **27**: 1087–1105.

McSaveney MJ. 2002. Recent rockfalls and rock avalanches in Mount Cook National Park, New Zealand. In *Catastrophic Landslides: Effects, Occurrence, and Mechanisms*, Evans SG, DeGraff JV (eds). Reviews in Engineering Geology XV. Geological Society of America: 35–70.

McSaveney MJ, Davies TR, Hodgson KA. 2000. A contrast in deposit style and process between large and small rock avalanches. In *Landslides in Research, Theory and Practice*, Bromhead E, Dixon N, Ibsen ML (eds). Proceedings 8th International Symposium on Landslides, 26–30 June, Cardiff. 1052–1058.

Norris RJ, Cooper AF. 1997. Erosional control on the structural evolution of a transpressional thrust complex on the Alpine Fault, New Zealand. *Journal of Structural Geology* **19**: 1323–1342.

Norris RJ, Cooper AF. 2000. Late Quaternary slip rates and slip partitioning on the Alpine Fault, New Zealand. *Journal of Structural Geology* **23**: 507–520.

Norris RJ, Cooper AF, Wright T, Berryman K. 2001. *Dating of past Alpine Fault rupture in South Westland*. EQC Report 99/341.

Owen LA, Sharma MC, Bigwood R. 1996. Landscape modification and geomorphological consequences of the 20th October 1991 earthquake and the July–August 1992 monsoon in the Garhwal Himalaya. *Zeitschrift für Geomorphologie Supplementband* N.F. **103**: 359–372.

Pain CF, Bowler JM. 1973. Denudation following the November 1970 earthquake at Madang, Papua New Guinea. *Zeitschrift für Geomorphologie Supplementband N.F.* **18**: 92–104.

Pearce AJ, Watson AJ. 1986. Effects of earthquake-induced landslides on sediment budget and transport over a 50-yr period. *Geology* **14**: 52–55.

Prebble WM. 1995. Landslides in New Zealand. Keynote paper. In *Landslides. Glissements de terrain*, Bell DH (ed.). Proceedings of the 6th International Symposium, 10–14 February 1992, Christchurch. Balkema: Rotterdam; 2101–2123.

Radbruch-Hall DH. 1978. Gravitational creep of rock masses on slopes. In *Rockslides and Avalanches 1*, Voight B (ed.). Elsevier: Amsterdam; 607–657.

Ramsay G. 2000. Otira Gorge rock avalanche. In *Landslides in Research, Theory and Practice*, Bromhead E, Dixon N, Ibsen ML (eds). Proceedings 8th International Symposium on Landslides, 26–30 June, Cardiff. 1274–1280.

Ries JB. 2000. The landslide in the Surma Khola Valley, High Mountain Region of the Central Himalaya in Nepal. *Physics and Chemistry of the Earth Part B* **25**: 51–57.

Schlunegger F. 2002. Impact of hillslope-derived sediment supply on drainage basin development in small watersheds at the northern border of the central Alps of Switzerland. *Geomorphology* **46**: 285–305.

Schmelzer RM. 2000. *Massenbewegungen im Hochgebirge: Talzuschub und Bergsturz im Annapurna Himal, Manang District, West Nepal*. Akademické nakladatelství: Brnol.

Shroder Jr JF, Bishop MP. 1998. Mass movement in the Himalaya: new insights and research directions. *Geomorphology* **26**: 13–35.

Simpson GDH, Cooper AF, Norris RJ. 1994. Late Quaternary evolution of the Alpine Fault zone at Paringa, South Westland, New Zealand. *New Zealand Journal of Geology and Geophysics* **37**: 49–58.

Soeters R, Van Westen CJ. 1996. Slope instability recognition, analysis, and zonation. In *Landslides: Investigation and Mitigation*, Turner AK, Schuster RL (eds). Special Report 247. Transportation Research Board, National Research Council: 129–177.

Stark CP, Hovius N. 2001. The characterization of landslide size distributions. *Geophysical Research Letters* **28**: 1091–1094.

Turnbull IM. 2000. *Geology of the Wakatipu Area*. 1:250 000 Geological Map 18. Institute of Geological and Nuclear Sciences: Lower Hutt.

Turnbull IM, Mortimer N, Craw D. 2001. Textural zones in the Haast Schist – a reappraisal. *New Zealand Journal of Geology and Geophysics* **44**: 171–183.

Walcott RI. 1998. Modes of oblique compression: late Cenozoic tectonics of the South Island of New Zealand. *Reviews of Geophysics* **36**: 1–26.

Wells A, Duncan RP, Stewart GH. 2001. Forest dynamics in Westland, New Zealand: The importance of large, infrequent earthquake-induced disturbance. *Journal of Ecology* **89**: 1006–1018.

White SR. 2002. The Siberia Fault Zone, northwest Otago, and kinematics of mid-Cenozoic plate boundary deformation in southern New Zealand. *New Zealand Journal of Geology and Geophysics* **45**: 271–287.

Whitehouse IE. 1983. Distribution of large rock avalanche deposits in the central Southern Alps, New Zealand. *New Zealand Journal of Geology and Geophysics* **26**: 272–279.

Whitehouse IE. 1986. Geomorphology of a compressional plate boundary, Southern Alps, New Zealand. In *International Geomorphology*, Gardiner V (ed.). John Wiley: Chichester; 897–924.

Whitehouse IE. 1988. Geomorphology of the central Southern Alps, New Zealand: the interaction of plate collision and atmospheric circulation. *Zeitschrift für Geomorphologie Supplementband N.F.* **69**: 105–116.

Whitehouse IE, Griffiths GA. 1983. Frequency and hazard of large rock avalanches in the central Southern Alps. *Geology* **11**: 331–334.

Wright CA. 1999. The AD 930 long-runout Round Top debris avalanche, Westland, New Zealand. *New Zealand Journal of Geology and Geophysics* **41**: 493–497.

Yetton MD, Wells A, Traylen NJ. 1998. *The Probability and Consequences of the Next Alpine Fault Earthquake*. EQC Research Project 95/193. Geotech Consulting Ltd: Christchurch.

